Supporting Information

Regulation of Local Chemistry in O3-type Layered Oxide Cathodes for Practical Sodium-Ion Batteries

Tongtong Huo,[a] Qian Yang,[a] Genliang Yu,[a] Mingyue Li,[a] Xuejie Bai,[a] Ting Lv,[a] Xiaobo Zhang,[a] Jie Xu,[a] Kai Liu,[a] Xunzhu Zhou,[b] Xin Tan, [b,c] Lin Li,*[b,c] Kaixiang Lei,*[a] and Shijian Zheng,*[a]

[a] T. Huo, Q. Yang, G. Yu, M. Li, X. Bai, T. Lv, X. Zhang, J. Xu, K. Liu, Dr. K. Lei, Prof. S. Zheng
Tianjin Key Laboratory of Materials Laminating Fabrication and Interface Control Technology, School of Materials Science and Engineering, Hebei University of Technology
Tianjin 300401, China
E-mail: kaixianglei@hebut.edu.cn; sjzheng@hebut.edu.cn

[b] Dr. X. Zhou, Dr. X. Tan, Prof. L. Li
Institute for Carbon Neutralization Technology, College of Chemistry and Materials Engineering, Wenzhou University
Wenzhou, Zhejiang 325035, China
E-mail: linli@wzu.edu.cn

[c] Prof. L. Li
Zhejiang Provincial Key Laboratory of Advanced Battery Materials and Technology, Wenzhou University
Technology Innovation Institute for Carbon Neutralization
Shanghai 200093, China

Experimental Procedures

Material Synthesis. The $NaNi_{0.25}Fe_{0.14}Mn_{0.3}Li_{0.1}Ti_{0.15}Cu_{0.03}Zn_{0.03}O_{1.94}F_{0.06}$ (HEO) was prepared using a simple solid-phase reaction. Specifically, reagents such as Na_2CO_3, NiO, Fe_2O_3, MnO_2, $LiOH·H_2O$, TiO_2, CuO, ZnO and NaF were mixed in a stoichiometric ratio and dispersed in 3 mL of anhydrous ethanol to form a homogeneous mixture. The mixture was then thoroughly ground in a planetary ball mill at a ball-to-material mass ratio of 6:1 and a speed of 900 rpm for 12 h. An excess of 5 wt.% of sodium carbonate and lithium hydroxide monohydrate was added to compensate for losses during high-temperature calcination. The paste-like mixture was dried in a ventilated oven at 80 °C for 1 h, and 0.6 g of the dried powder was transferred to a muffle furnace. It was heated at a rate of 5 °C min^{-1} to 450 °C for calcination of 3 h, then further heated at the same rate to 850 °C for calcination of 12 h, and finally quickly transferred to an argon-filled glove box for subsequent use. The synthesis methods of NFM and single-doped samples are similar with different stoichiometric ratio.

Materials Characterization. The crystal structure was characterized by powder X-ray diffraction (XRD) using a Rigaku SmartLab 9 kW instrument with Cu Kα radiation (λ=1.54 Å) over a 2θ range of 10-80°, at a scan speed of 6° min^{-1} and a step size of 0.02°. In situ X-ray diffraction tests were conducted in a specially designed cell, with charge-discharge cycles at a current density of 30 mA g^{-1} within a voltage range of 2.0-4.2 V, collecting data every 10 minutes. The particle morphology and size of the samples were characterized by scanning electron microscopy (SEM, JEOL JSM7610F). High-resolution transmission electron microscopy (HRTEM) images and energy dispersive spectroscopy (EDS) spectra were obtained on a JEM-2100F. The crystal structure images were obtained via spherical aberration corrected scanning transmission electron microscope (AC-STEM) combined with high-angle annular dark-field (HAADF). The chemical composition of the prepared materials was analyzed using inductively coupled plasma optical emission spectroscopy (ICP-OES) and fluoride-ion selective electrode menthod (ISE). X-ray photoelectron spectroscopy (XPS) spectra were collected using Thermo Scientific Nexsa G2 to analyze the elemental valence states and chemical composition. The spectrometer was equipped with an Al Kα X-ray source, a 15 kV X-ray beam (analysis area: 200 μm×200 μm), and Ar^+ etching. All spectra were calibrated using the C 1s photoemission peak at 284.8 eV. X-ray absorption spectroscopy was recorded using an

easyXAFS 300+. Differential electrochemical mass spectrometry (DEMS) (QMG200, Shanghai Linglu) was used to investigate gas evolution during charging. Electron paramagnetic resonance (EPR) spectra were recorded on a Bruker EMXplus-6/1 spectrometer. Raman spectroscopy measurements were performed on a LabRAM HR spectrometer with a 523 nm excitation laser.

The configurational entropy (S_{config}) is calculated according to the following equation:[1]

$$S_{config} = -R\left[\left(\sum_{i=1}^{n} x_i \ln x_i\right)_{cation-site} + \left(\sum_{j=1}^{m} x_j \ln x_j\right)_{anion-site}\right]$$

where R stands for the gas constant, x_i expresses the concentration of component i in cations, x_j indicates the concentration of component j in anions, n represents the number of cation species, m signifies the number of anion species. The configuration entropy calculation process for NFM and HEO is as follows:

(1) $NaNi_{0.4}Fe_{0.2}Mn_{0.4}O_2$ (NFM):

$S_{config,cation}$ = -R[(0.4ln0.4+0.2ln0.2+0.4ln0.4)]≈1.055R

$S_{config,anion}$ = 0

$S_{config,total}$ = $S_{config,cation}$+ $S_{config,anion}$ =1.055R

(2) $NaNi_{0.25}Fe_{0.14}Mn_{0.3}Li_{0.1}Ti_{0.15}Cu_{0.03}Zn_{0.03}O_{1.94}F_{0.06}$ (HEO):

$S_{config,cation}$ = -R[(0.25ln0.25+0.14ln0.14+0.3ln0.3+0.1ln0.1+0.15ln0.15+0.03ln0.03+0.03ln0.03)]≈1.708R

$S_{config,anion}$ = -R[(0.97ln0.97+0.03ln0.03)]≈0.135R

$S_{config,total}$ = $S_{config,cation}$+ $S_{config,anion}$ =1.843R

Electrochemical Measurement. CR2032-type coin cells were assembled in an argon-filled glove box with a Button Cell Sealing Machine (MSK-160E). Sodium discs (12 mm in diameter) were obtained by rolling and cutting fresh sodium metal blocks. The cathode material, Super-P, and PVdF were mixed in a weight ratio of 8:1:1, and coated onto aluminum foil with a thickness of 100 micrometers. The coated foil was then dried under vacuum at 80 °C for 12 h, followed by cutting into cathode electrodes with a diameter of 12 mm. The anode electrodes were prepared similarly to the cathode, employing hard carbon (HC) and copper foil as the active material and current collector, respectively. In half cells, sodium metal was used as the anode, glass fiber filter

paper was used as the separator, and 1.0 M $NaClO_4$ in propylene carbonate: ethyl methyl carbonate: ethylene carbonate (1:1:1, v/v/v) with 2 wt.% fluoroethylene carbonate was used as the electrolyte. In full cells, HC was employed as the anode and pre-activated prior to assembly, with the N/P ratio controlled at 1.1:1. Electrochemical long-term cycling tests at constant and varying rates were carried out on the LAND Battery Test System. Coin cells were evaluated over a voltage range of 2.0-4.2 V for long-term cycling at 1.0 C (150 mA g^{-1}), 5.0 C, 10.0 C and 20.0 C. The rate performance of coin cells was tested in steps of 0.2 C, 0.5 C, 1.0 C, 5.0 C, 10.0 C, 20.0 C and 0.2 C. The cyclic voltammetry (CV) and electrochemical impedance spectroscopy (EIS) were measured on a ChenHua electrochemical workstation (CHI660E, CH Instruments Inc.). CV was tested at a scan rate of 0.1 mV s^{-1} for first three cycles in the voltage range of 2.0-4.2 V. Additionally, electrochemical CV curves were assessed at varying scan rates of 0.1, 0.2, 0.4, 0.6, 0.8, and 1.0 mV s^{-1}. EIS was performed in a scan frequency range from 10^5 Hz to 10^{-1} Hz at open circuit potential with an amplitude of 5.0 mV.

For GITT measurements, coin cells were charged at a current of 15 mA g^{-1} for 10 min, followed by a rest period of 120 min. The diffusion coefficient is calculated using the following formula:

$$D = \frac{4}{\pi\tau}\left(\frac{m_B V_M}{M_B S}\right)^2\left(\frac{\Delta E_S}{\Delta E_\tau}\right)^2$$

Here, m_B, M_B, and V_M represent the mass, relative molar weight, and molar volume of the synthesized sample, respectively. S is the geometric area of the electrode. ΔE_s and ΔE_τ refer to the steady-state voltage change and the transient voltage change, respectively.

The diffusion coefficients Na^+ were calculated by fitting the CV curves at different scan rates by the Randles Sevcik equation, as shown below:

$$D^{0.5} = \frac{1}{268700 \times A \times C \times n^{1.5}} \times \frac{I_p}{v^{0.5}}$$

Where I_p is the normalised peak current (A mg^{-1}), n is the number of electrons transferred during the redox reaction, A is the geometrical surface area of the electrode (cm^2), C is the molar concentration of sodium ions (mol cm^{-3}), v is the scanning rate (V s^{-1}), and D is the sodium ion diffusion coefficient (cm^2 s^{-1}).

Theoretical calculation. The hexagonal unit cell ($\gamma = 120°$) was transformed into an orthogonal supercell through lattice vector redefinition and supercell expansion. The unit cell of $NaFeO_2$ is specifically $Na_3Fe_3O_6$. After lattice redefinition and supercell expansion, the final composition is $Na_{36}Ni_{15}Fe_7Mn_{14}O_{72}$ and $Na_{36}Ni_9Fe_5Mn_{11}Li_4Ti_5Cu_1Zn_1O_{70}F_2$. All density functional theory (DFT) calculations were performed by using the projector augmented wave method as implemented in the VASP.[2] The electron exchange-correlation interactions were parameterized by the generalized gradient approximation (GGA) with the Perdew-Burke-Ernzerhof (PBE).[3-4] The Brillouin zone was sampled by the Γ-centered k-mesh with a resolution of $2\pi \times 0.04$ Å^{-1} for geometry optimization and $2\pi \times 0.02$ Å^{-1} for electronic structure calculation. The plane-wave energy cutoff was set to 500 eV, and the convergence tolerance for residual force and energy on each atom during structure relaxation were set to 0.02 eV/Å and 10^{-5} eV, respectively. The Hubbard U correction method was employed, with $U_{(Ni\ 3d)} = 6.2$ eV, $U_{(Fe\ 3d)} = 4.3$ eV, $U_{(Mn\ 3d)} = 3.9$ eV, $U_{(Ti\ 3d)} = 4.2$ eV, $U_{(Zn\ 3d)} = 4.0$ eV, and $U_{(Cu\ 3d)} = 7.0$ eV as reported in previous studies.[5-8] Van der Waals interaction (DFT-D3 method with Becke-Jonson damping) was incorporated.[9-10] The VASPKIT code is used to finish the pre- and post-processing of the calculation results.[11] Structural and charge density visualization was conducted utilizing the VESTA software.[12] The crystal orbital Hamilton population (COHP) analysis was performed using the LOBSTER 5.1.0 package.[13]

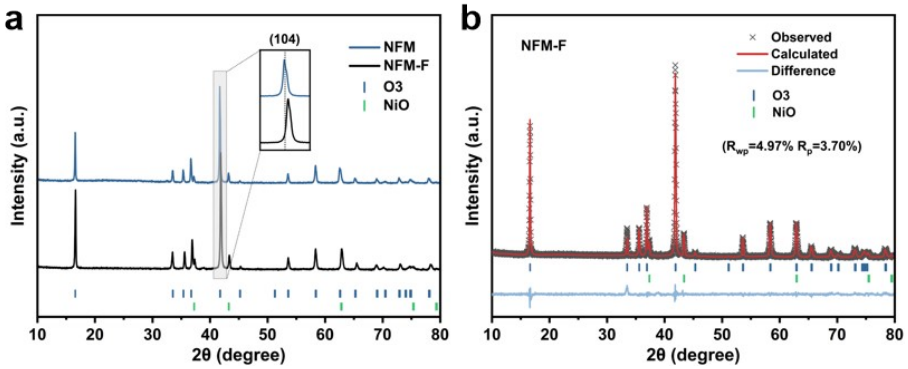

Figure S1. XRD patterns and corresponding Rietveld refinement of NFM-F.

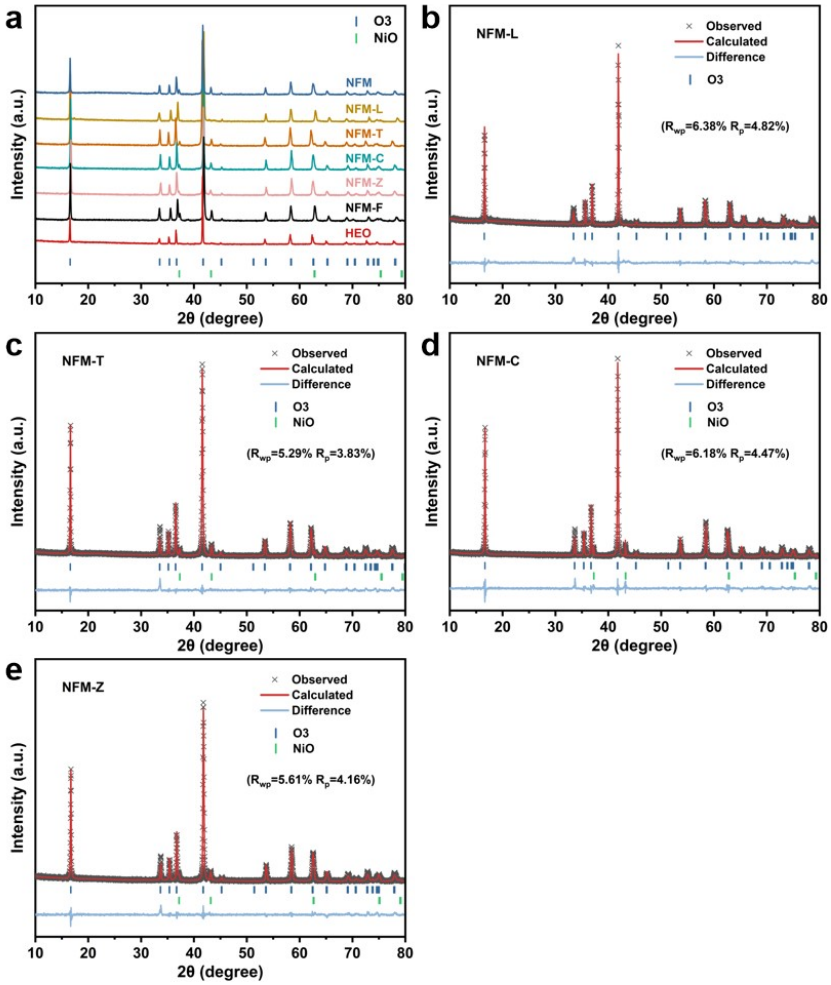

1

2**Figure S2.** XRD patterns and corresponding Rietveld refinement of the comparative samples.

1

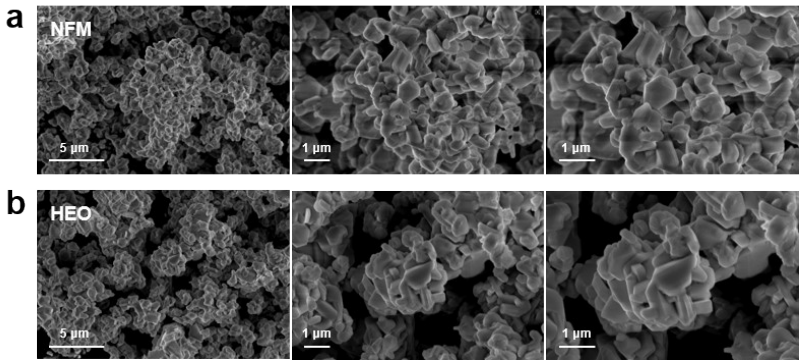

2**Figure S3.** SEM images of (a) NFM and (b) HEO.

1

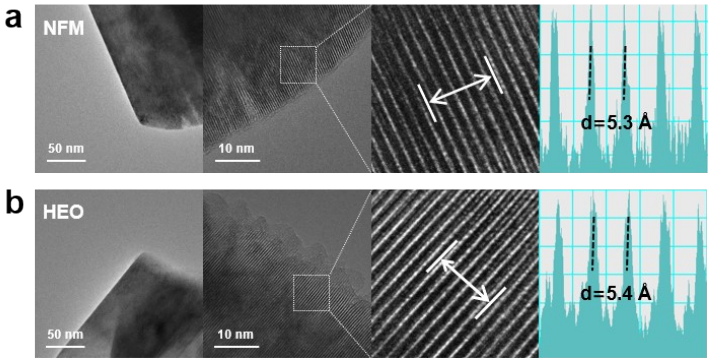

2**Figure S4.** HRTEM images of (a) NFM and (b) HEO.

1 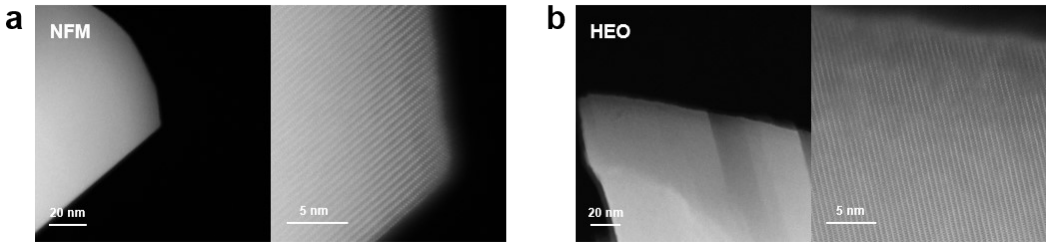

2**Figure S5.** AC-HAADF-STEM images of (a) NFM and (b) HEO.

1

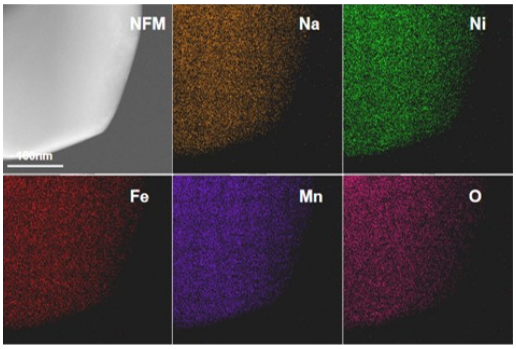

2**Figure S6.** Energy dispersive spectroscopy elemental mappings of NFM.

1

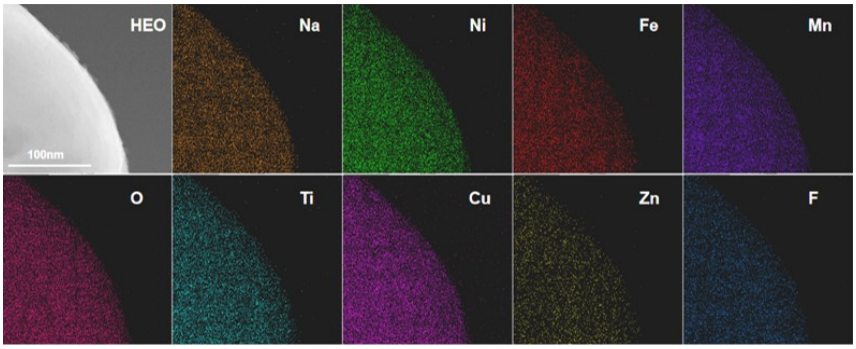

2**Figure S7.** Energy dispersive spectroscopy elemental mappings of HEO.

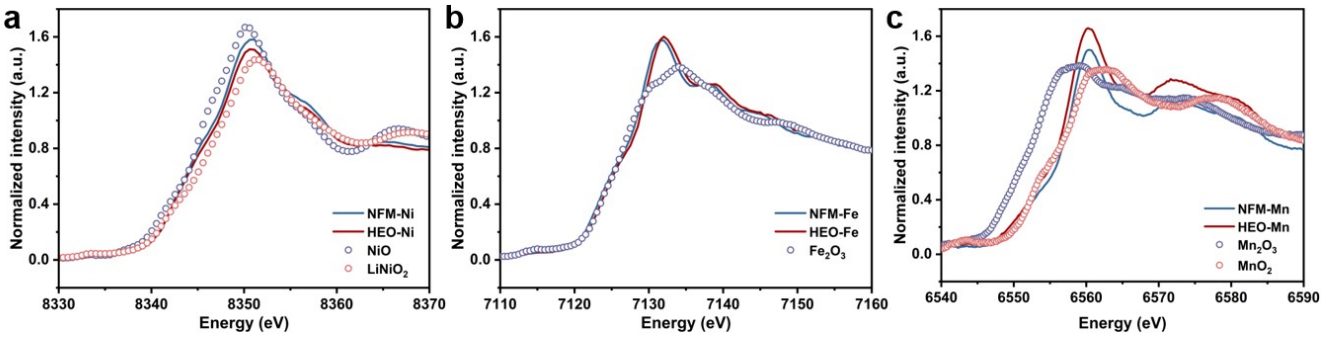

Figure S8. XANES spectra of the (a) Ni K-edge, (b) Fe K-edge and (c) Mn K-edge.

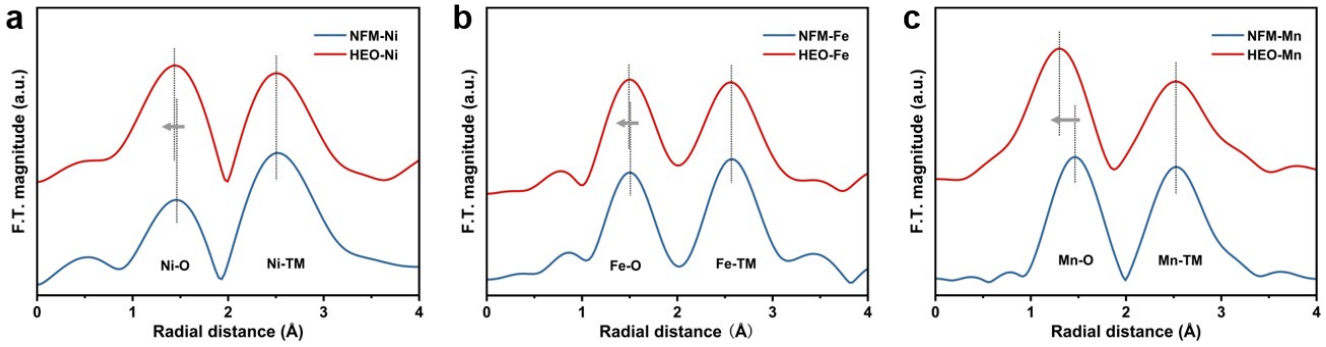

Figure S9. EXAFS spectra of the (a) Ni K-edge, (b) Fe K-edge and (c) Mn K-edge.

1

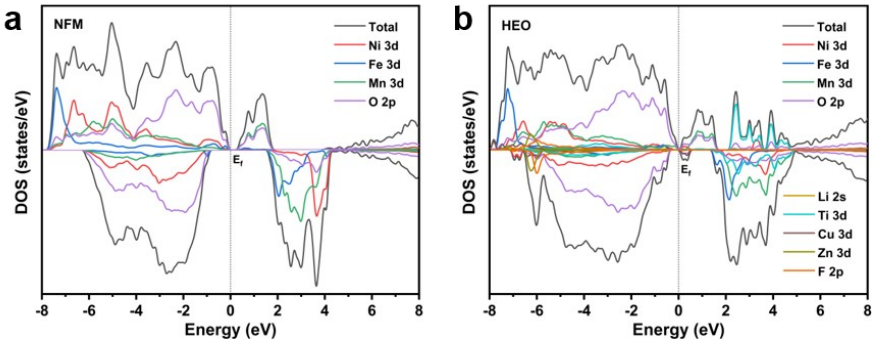

2**Figure S10.** Total DOS and projected DOS of (a) NFM and (b) HEO.

1

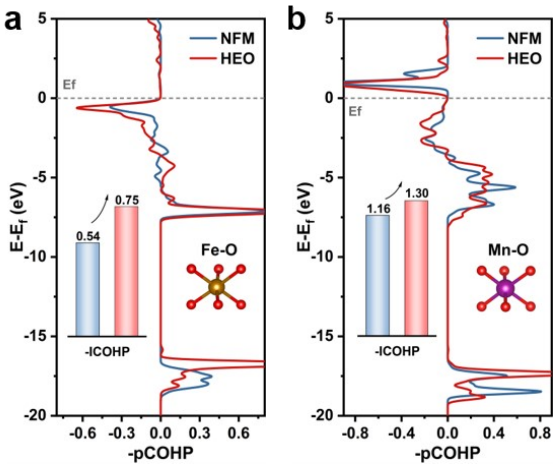

2**Figure S11.** COHP results of (a) Fe-O and (b) Mn-O bonds in NFM and HEO.

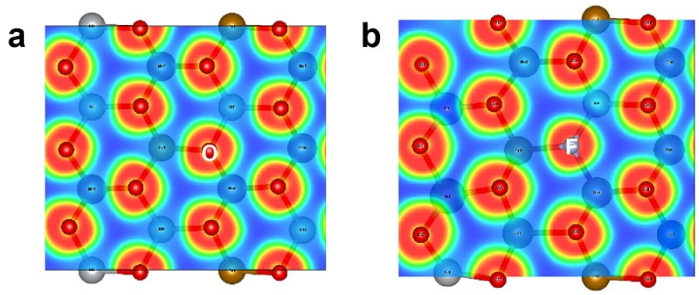

Figure S12. ELF of the valence electron in O-layer viewed along the [001] direction.

1

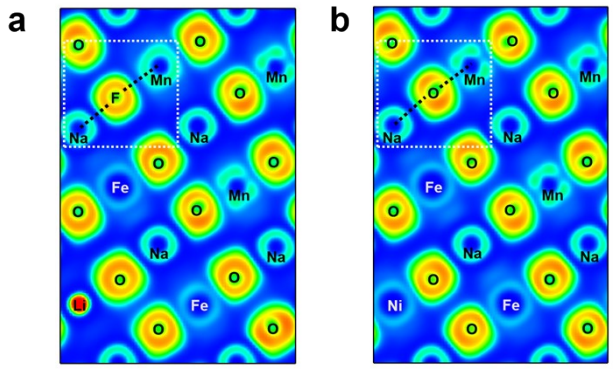

2**Figure S13.** ELF of the valence electron viewed along the [100] direction.

1 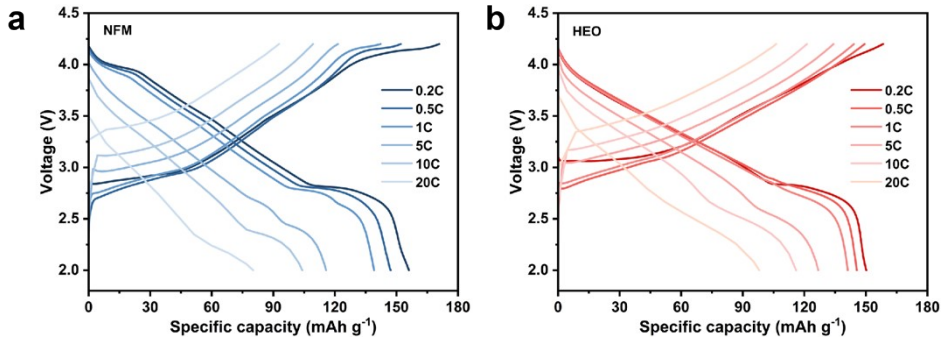

2**Figure S14.** Galvanostatic charge/discharge curves of (a) NFM and (b) HEO from 0.2 to 20.0 C.

1

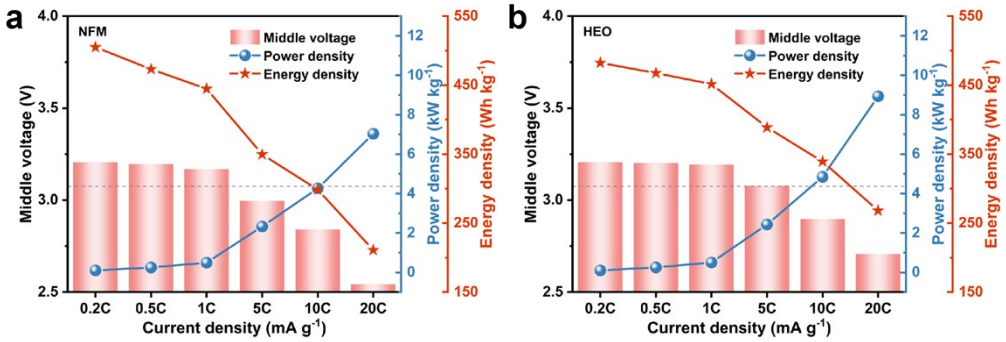

2**Figure S15.** The middle voltage, energy density, and power density of (a) NFM and (b) HEO.

1

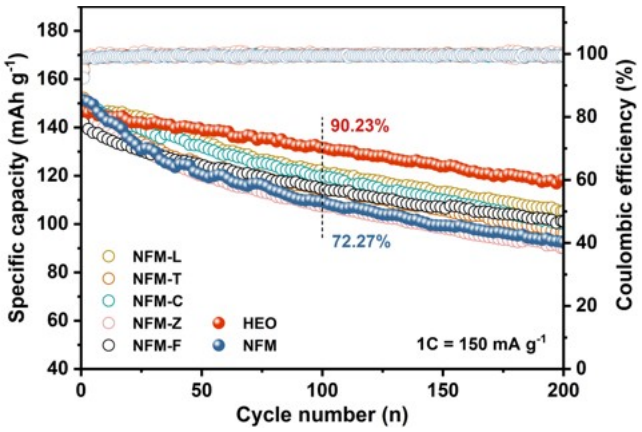

2**Figure S16.** Long-term cycling performance of the comparative samples at 1.0 C.

1

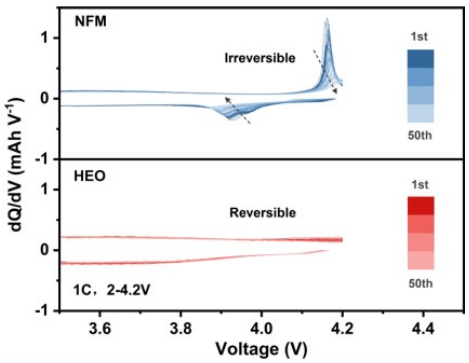

2**Figure S17.** The dQ/dV curves of NFM and HEO from the 1st to the 50th cycle at 1.0 C.

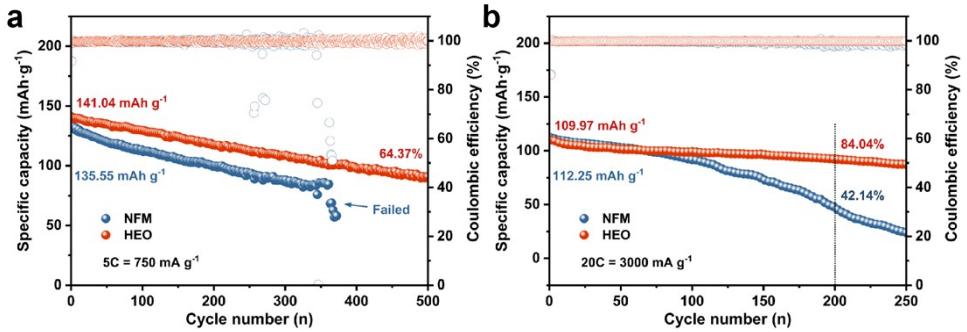

Figure S18. Long-term cycling performance of NFM and HEO at (a) 5.0 C and (b) 20.0 C.

1

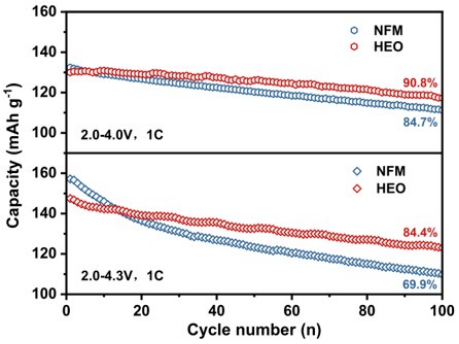

2**Figure S19.** Long-term cycling performance of NFM and HEO at 2.0-4.0 V and 2.0-4.3 V.

1

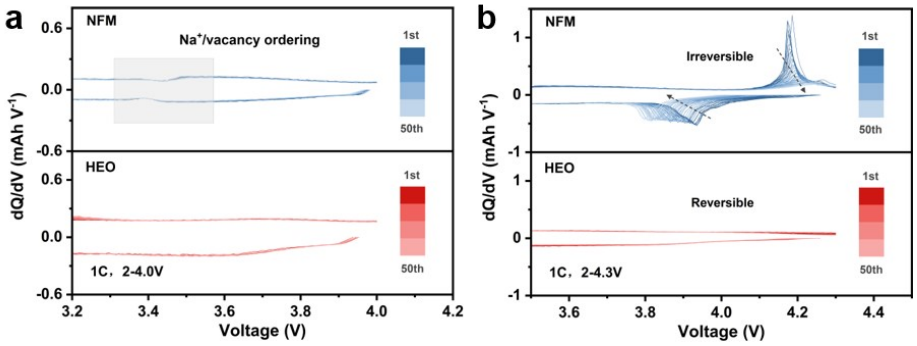

2**Figure S20.** The dQ/dV curves of NFM and HEO at a cut-off voltage of (a) 4.0 V and (b) 4.3 V.

1

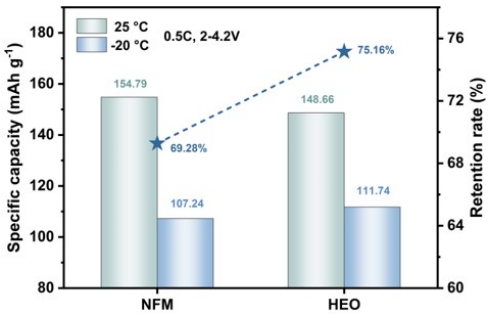

2**Figure S21.** Specific capacity comparison between NFM and HEO at 0.5 C under 25 °C and -20 °C.

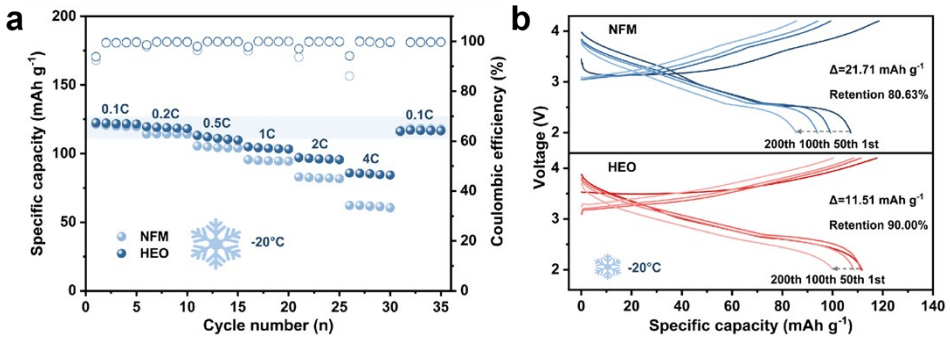

Figure S22. (a) Rate performance and (b) cycling performance of NFM and HEO at -20 °C low temperature.

1

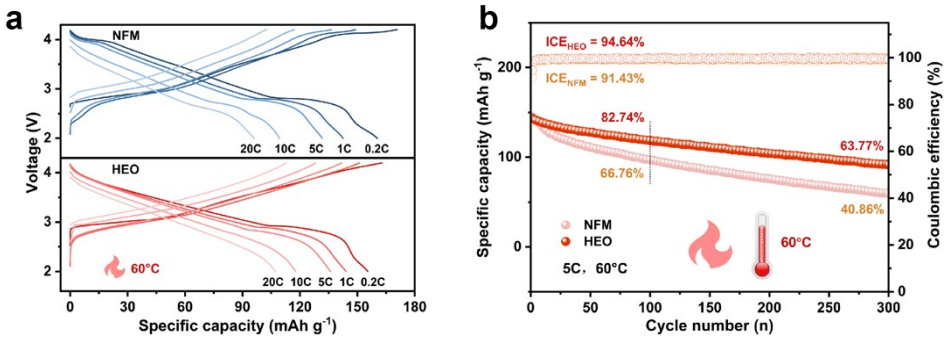

2**Figure S23.** (a) Rate performance and (b) cycling performance of NFM and HEO at 60 °C high temperature.

1

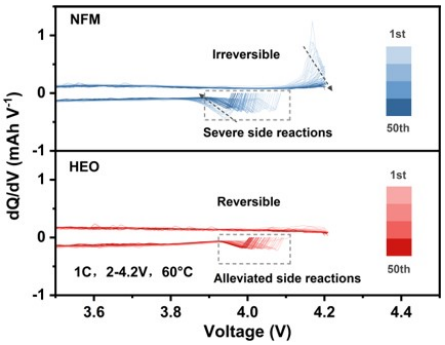

2**Figure S24.** The dQ/dV curves of NFM and HEO from the 1st to the 50th cycle at 60 °C high temperature.

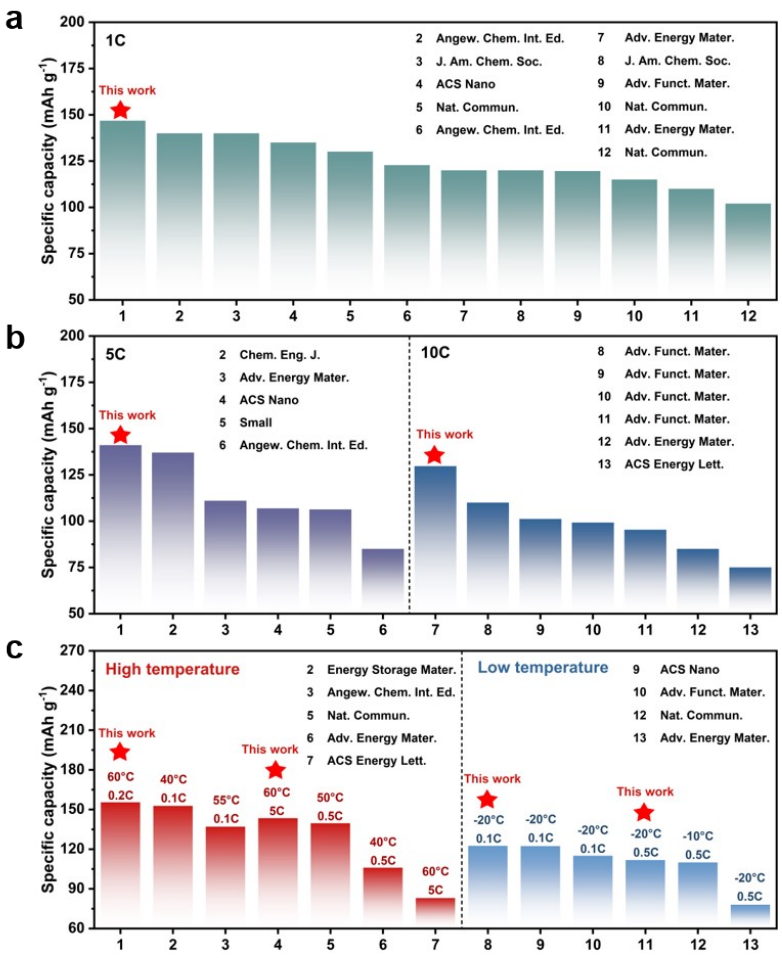

Figure S25. Comparison of half-cell performance with reported literatures over the past three years.

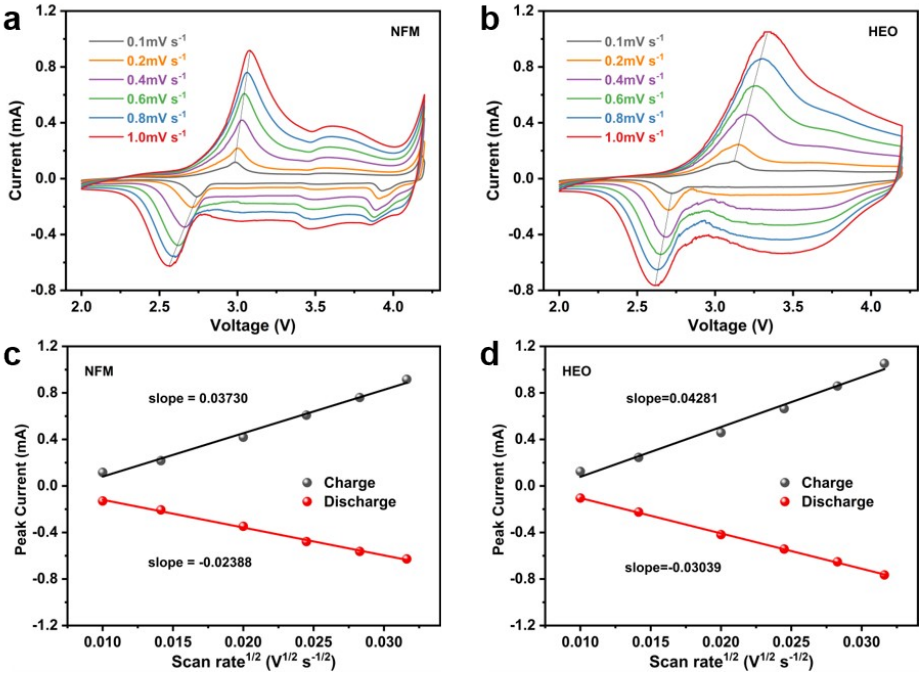

Figure S26. CV curves of (a) NFM and (b) HEO at different scan rates. The plot of the peak current of (c) NFM and (d) HEO as a function of the square root of scan rates.

1 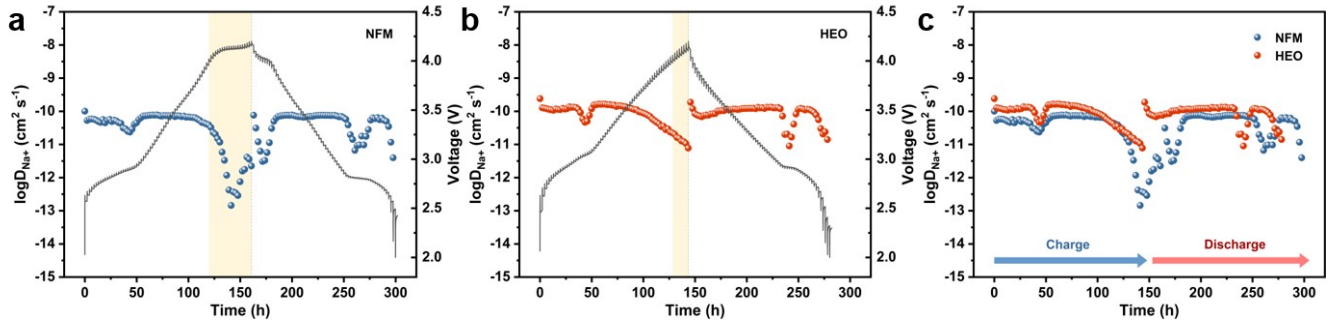

2**Figure S27.** GITT curves of (a) NFM, (b) HEO, and (c) their comparison at 0.1 C.

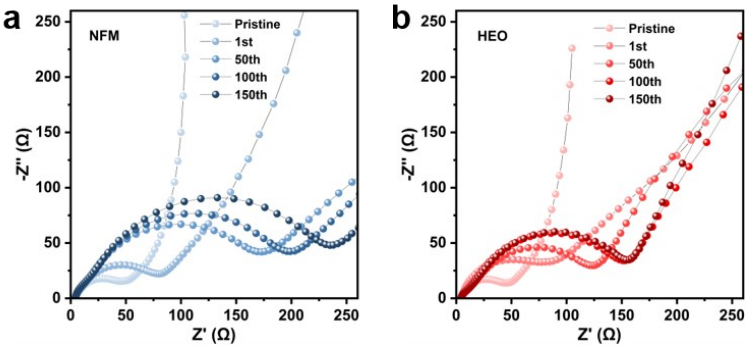

Figure S28. EIS results of (a) NFM and (b) HEO before and after cycles.

1

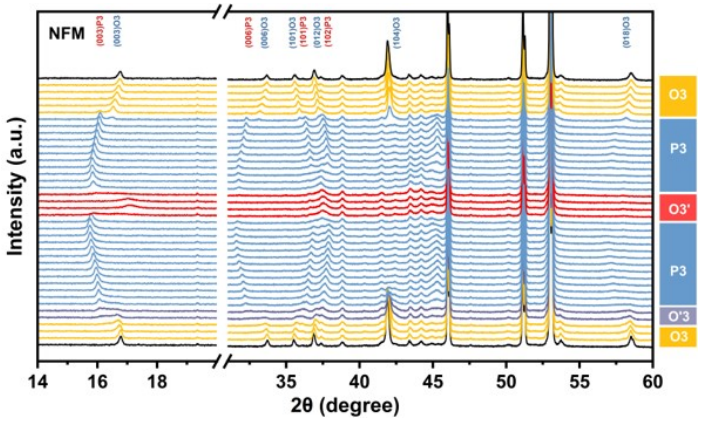

2**Figure S29.** *In-situ* XRD patterns of NFM during the initial cycle at 0.2 C.

1

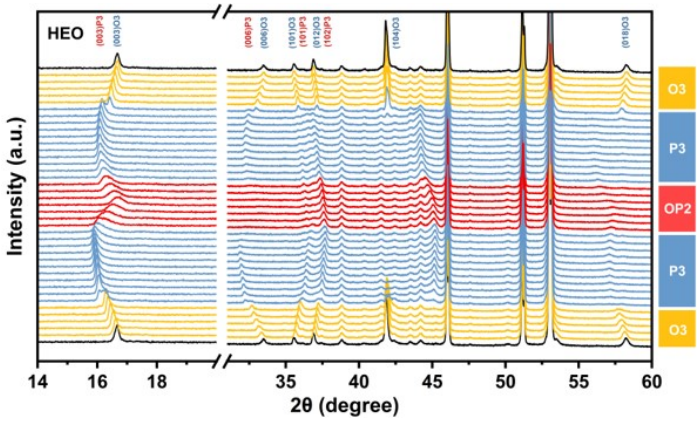

2**Figure S30.** *In-situ* XRD patterns of HEO during the initial cycle at 0.2 C.

1

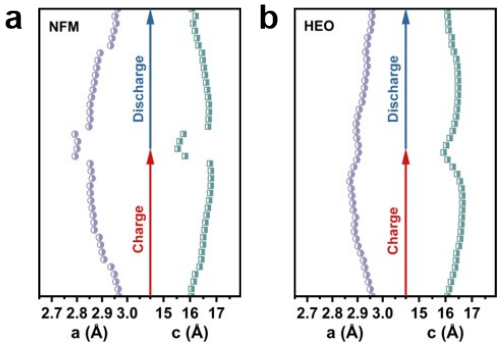

2**Figure S31.** The corresponding lattice parameter (*a* and *c*) changes of (a) NFM and (b) HEO during the initial

3cycle.

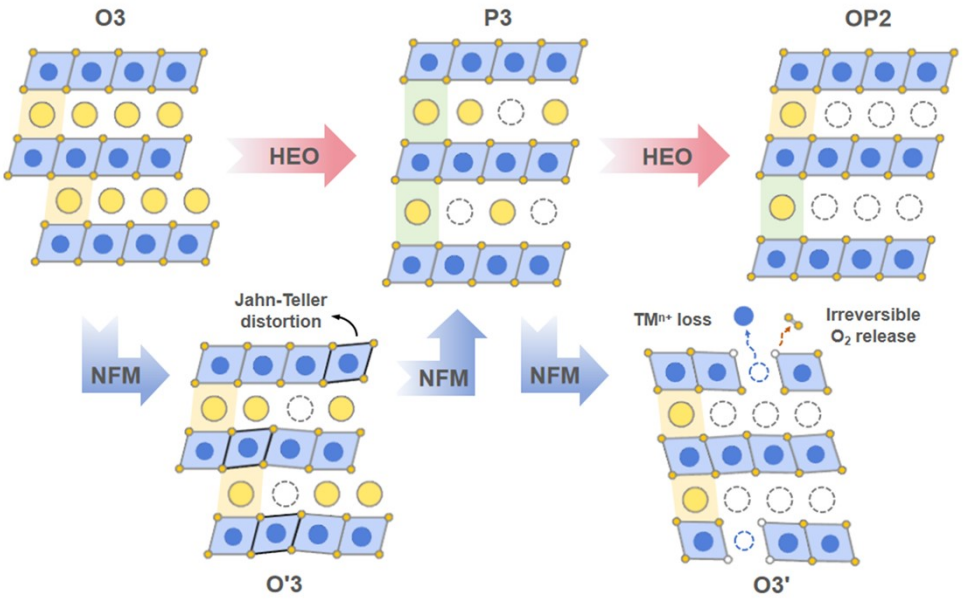

Figure S32. Schematic diagram of phase transitions of NFM and HEO during charge/discharge process.

1

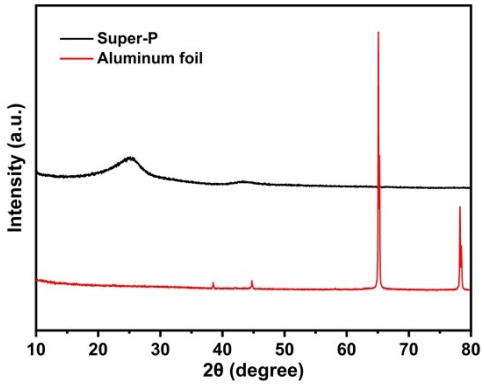

2**Figure S33.** XRD patterns of Super-P and aluminum foil.

1

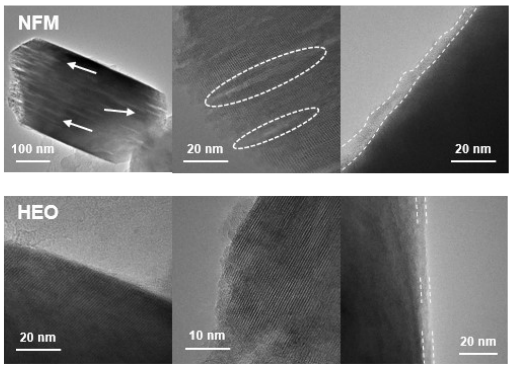

2**Figure S34.** TEM images of (a) NFM and (b) HEO after 300 cycles.

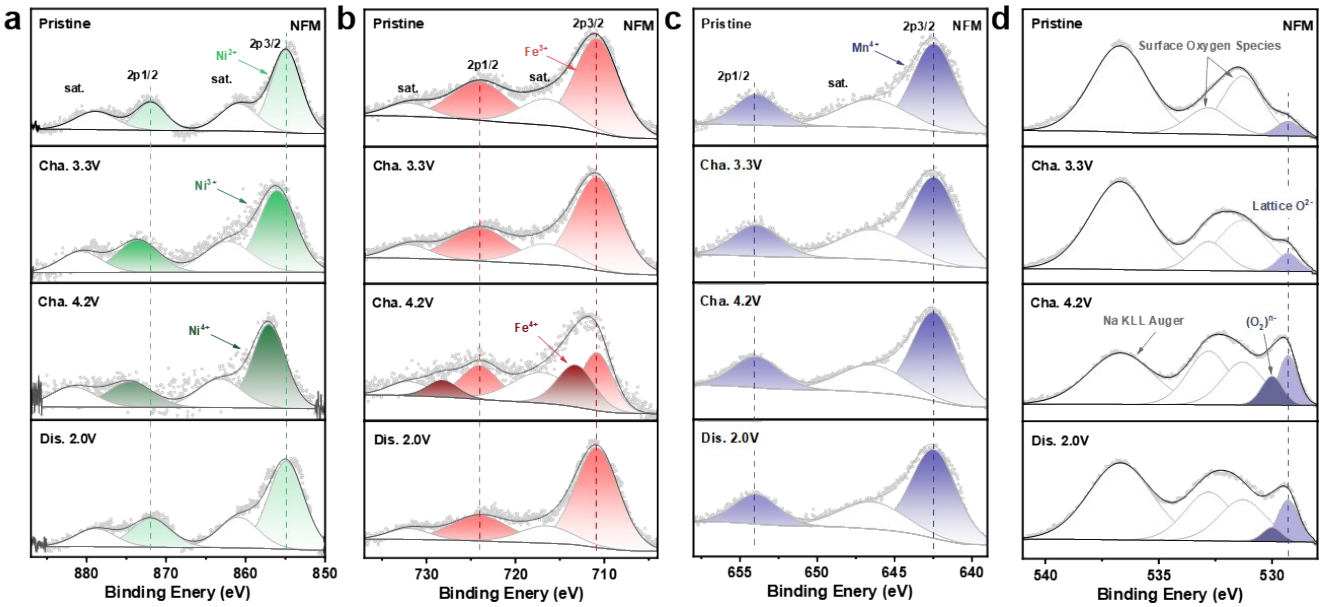

1

2**Figure S35.** XPS spectra of (a) Ni 2p, (b) Fe 2p, (c) Mn 2p, and (d) O 1s in NFM at various charge/discharge

3states during the initial cycle.

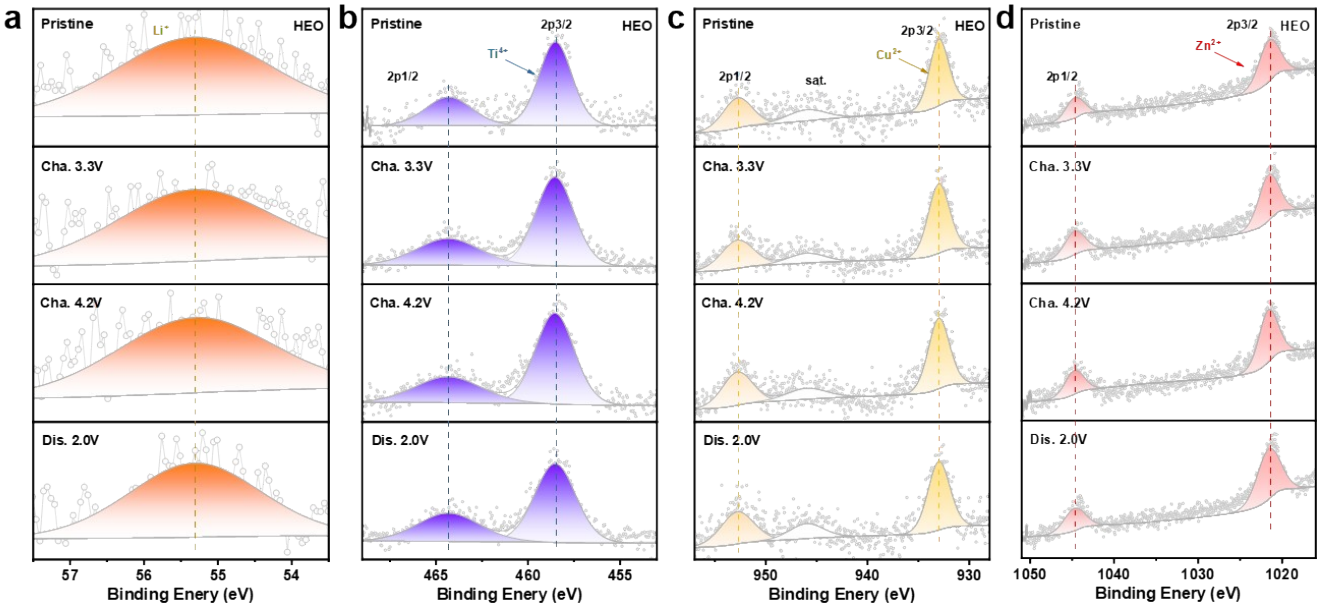

1

2**Figure S36.** XPS spectra of (a) Li 1s, (b) Ti 2p, (c) Cu 2p, and (d) Zn 2p in HEO at various charge/discharge

3states during the initial cycle.

1

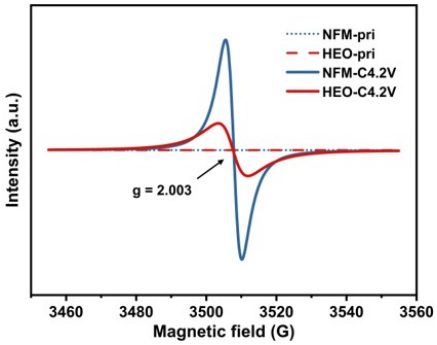

2**Figure S37.** EPR results at various charge/discharge states during the initial cycle.

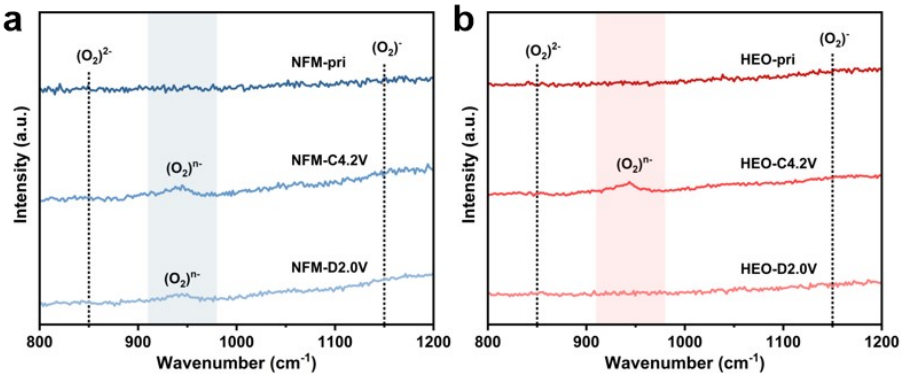

Figure S38. Raman spectroscopy at various charge/discharge states.

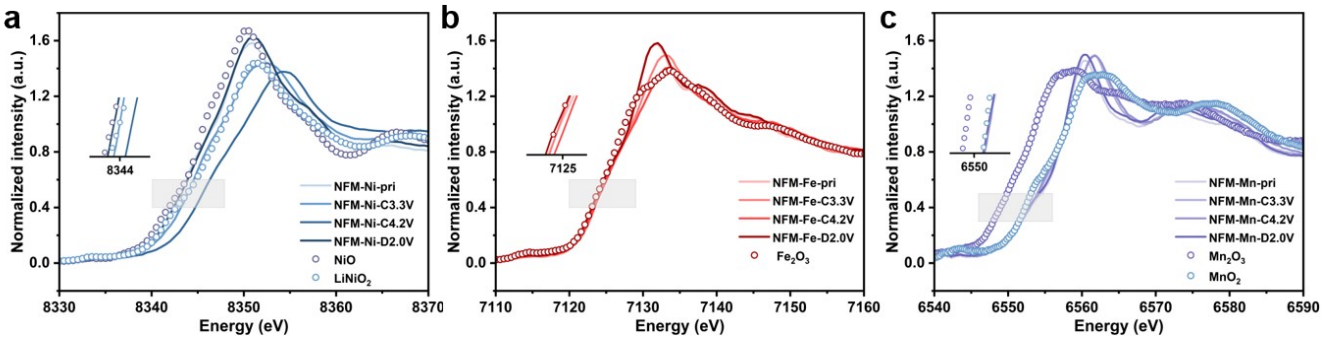

Figure S39. XANES spectra of (a) Ni-K-edge, (b) Fe K-edge, and (c) Mn K-edge of NFM at various charge/discharge states during the initial cycle.

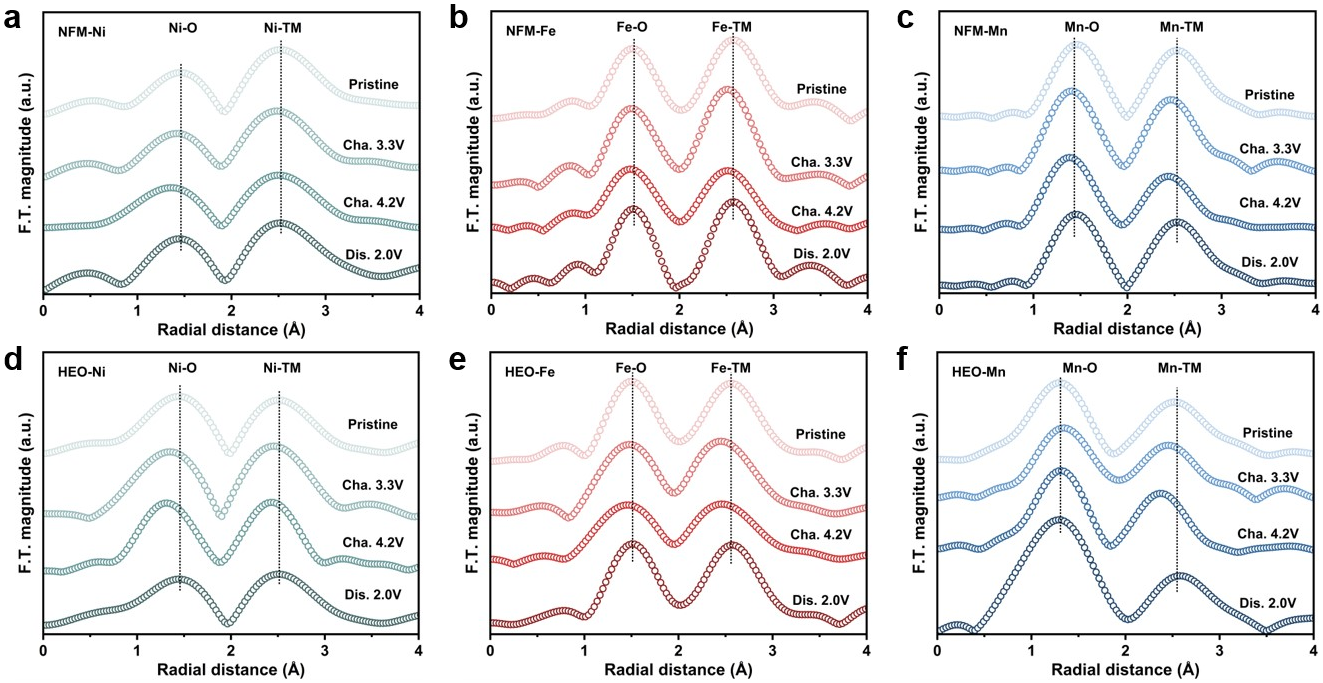

Figure S40. Ni, Fe, and Mn K-edge FT-EXAFS spectra of (a-c) NFM and (d-f) HEO at various charge/discharge states during the initial cycle.

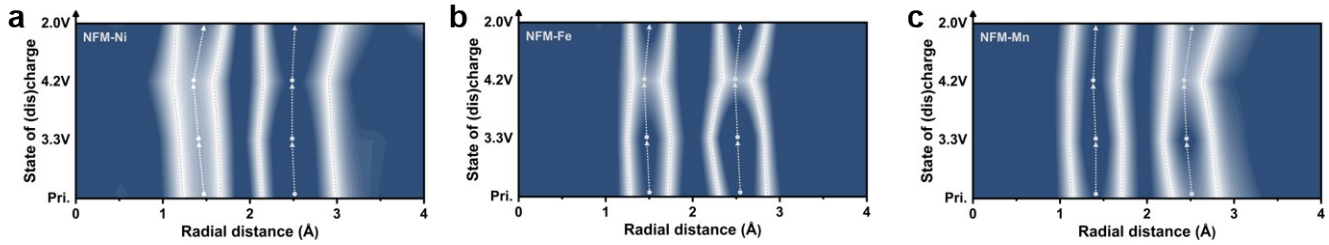

Figure S41. Contour maps of (a) Ni, (b) Fe, and (c) Mn K-edge FT-EXAFS spectra of NFM.

1

2**Figure S42.** Comparison of bond lengths between (a) Na-O bonds in NFM and (b) Na-F bonds in HEO.

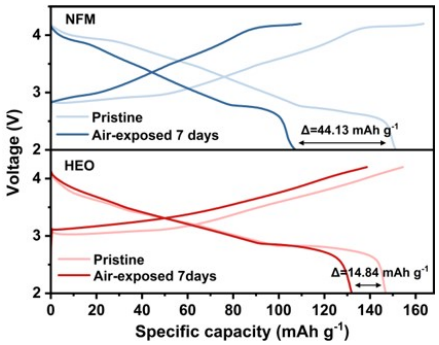

1

2**Figure S43.** Initial charge/discharge curves of NFM and HEO before and after air exposure at 1.0 C.

1 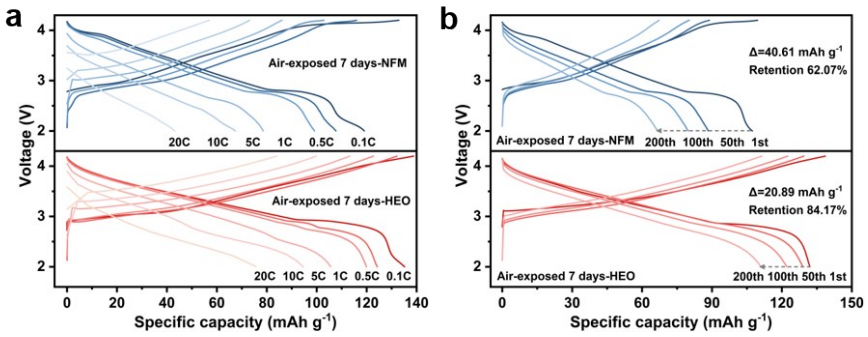

2**Figure S44.** (a) Rate performance and (b) cycling performance of NFM and HEO after air exposure.

1

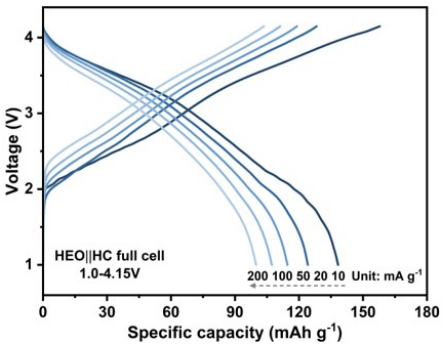

2

3**Figure S45.** Rate performance of the HEO||HC full cell.

1

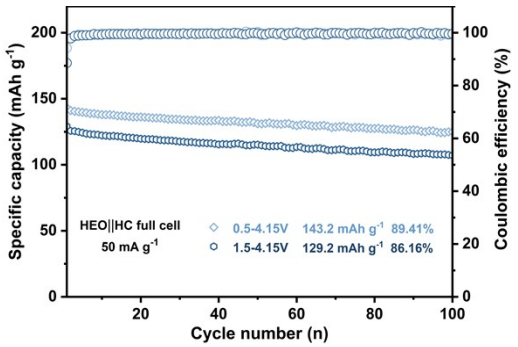

2**Figure S46.** Long-term cycling performance of the HEO||HC full cell at different voltage ranges.

Table S1. XRD refinement results of the comparative samples.

Parameter	a=b (Å)	c (Å)	V (Å^3)	$d_{(O\text{-}TM\text{-}O)}$ (Å)	$d_{(O\text{-}Na\text{-}O)}$ (Å)	$\Delta_{d(O\text{-}Na\text{-}O)}$ (Å)
NFM	2.9675	16.0360	122.2985	2.1872	3.1581	0
NFM-L	2.9511	16.1111	121.5116	2.1974	3.1729	+0.0148
NFM-T	2.9891	16.0620	124.2853	2.1907	3.1632	+0.0051
NFM-C	2.9748	16.0336	122.8822	2.1869	3.1577	-0.0004
NFM-Z	2.9786	16.0252	123.1301	2.1857	3.1560	-0.0021
NFM-F	2.9594	16.0613	121.8199	2.1801	3.1737	+0.0156
HEO	2.9797	16.0949	123.7562	2.1952	3.1697	+0.0116

Table S2. Crystallographic and Rietveld refinement data of NFM.

NFM (R-3m)		R_{wp}=5.19%, R_p = 3.16%			
Atom	Site	x	y	z	Occ
Na	3a	0	0	0.000	0.997
Ni	3b	0	0	0.500	0.398
Fe	3b	0	0	0.500	0.197
Mn	3b	0	0	0.500	0.400
O	6c	0	0	0.234	1.000

Table S3. Crystallographic and Rietveld refinement data of HEO.

HEO (R-3m)		R_{wp}=6.82%, R_p = 5.04%			
Atom	Site	x	y	z	Occ
Na	3a	0	0	0.000	0.995
Ni	3b	0	0	0.500	0.247
Fe	3b	0	0	0.500	0.139
Mn	3b	0	0	0.500	0.301
Li	3b	0	0	0.000	0.100
Ti	3b	0	0	0.500	0.148
Cu	3b	0	0	0.500	0.030
Zn	3b	0	0	0.500	0.030
O	6c	0	0	0.234	0.970
F	6c	0	0	0.234	0.030

Table S4. XRD refinement results of NFM and HEO.

Parameter	NFM	HEO
a (Å)	2.9675	2.9797
b (Å)	2.9675	2.9797
c (Å)	16.0360	16.0949
V (Å^3)	122.2985	123.7562
$d_{(O\text{-}TM\text{-}O)}$ (Å)	2.1872	2.1952
$d_{(O\text{-}Na\text{-}O)}$ (Å)	3.1581	3.1697
$V_{Octahedron}$ (Å^3)	16.0569	16.2482
$V_{Tetrahedron}$ (Å^3)	4.0142	4.0621

Table S5. ICP-OES and ISE results of NFM and HEO.

Theoretical chemical composition	Composition from ICP								
Materials	Na	Ni	Fe	Mn	Li	Ti	Cu	Zn	F
$NaNi_{0.4}Fe_{0.2}Mn_{0.4}O_2$	0.992	0.414	0.201	0.390	N/A	N/A	N/A	N/A	N/A
$NaNi_{0.25}Fe_{0.14}Mn_{0.3}Li_{0.1}Ti_{0.15}Cu_{0.03}Zn_{0.03}O_{1.94}F_{0.06}$	0.996	0.266	0.147	0.300	0.097	0.151	0.030	0.031	0.059

Table S6. Summary of the electrochemical performance (cycling stability) of layered oxides for sodium-ion batteries.

Temperature	Materials	Voltage region (V)	Capacity decay per cycle, Cycle number, Current density (mA g^{-1})	Ref.
Room temperature	O3-$NaNi_{0.3}Mn_{0.5}Fe_{0.05}Li_{0.05}Ti_{0.05}Cu_{0.05}O_2$	2-4.2 V	0.1085%, 200, 150	Adv. Energy Mater. 2025[14]
	O3-$NaNi_{1/3}Mn_{1/3}Fe_{1/3}O_2$ (Annealing)	2-4.2 V	0.1795%, 200, 100	Energy Storage Mater. 2025[15]
	O3-$Na[Ni_{1/3}Fe_{1/3}Mn_{1/3}]_{0.99}Sc_{0.01}O_2$	2-4.2 V	0.18%, 50, 130	Adv. Funct. Mater. 2024[16]
	O3-$Na_{0.9}Ni_{0.32}Zn_{0.08}Fe_{0.1}Mn_{0.3}Ti_{0.2}O_2$	2-4.2 V	0.107%, 100, 150	Angew. Chem. Int. Ed. 2024[17]
	O3-$NaNi_{0.3}Cu_{0.1}Fe_{0.2}Mn_{0.3}Ti_{0.1}O_2$	2-4.2 V	0.14%, 100, 140	Nat. Energy 2024[18]
	O3-$NaNi_{0.5}Mn_{0.48}La_{0.02}O_2$	2-4.2 V	0.157%, 100, 120	Adv. Funct. Mater. 2025[19]
	O3-$NaNi_{0.33}Fe_{0.33}Mn_{0.31}Sn_{0.02}O_2$	2-4.0 V	0.0995%, 200, 180; 0.108%, 200, 750	Adv. Funct. Mater. 2024[20]
	P2-$Na_{0.67}Mn_{0.011}[Mg_{0.1}\square_{0.07}Mn_{0.83}]O_2$	2-4.35 V	0.135%, 100, 140	Nat. Commun. 2025[21]
	O3-$NaCu_{0.1}Ni_{0.25}Co_{0.15}Mn_{0.35}$-$Li_{0.05}Ti_{0.05}Sn_{0.05}O_2$	2-4.4 V	0.099%, 100, 150	Angew. Chem. Int. Ed. 2025[22]
	P2/O3-$Na_{0.7}Ni_{0.2}Fe_{0.2}Mn_{0.5}Zn_{0.1}O_2$	2.4-4.5 V	0.0947%, 300, 600	ACS Nano 2024[23]
	O3-$Na_{2/3}Li_{1/6}Fe_{1/6}Co_{1/6}Ni_{1/6}Mn_{1/3}O_2$	2-4.5 V	0.121%, 300, 750	Adv. Energy Mater. 2022[24]
	O3-$NaNi_{1/3}Fe_{1/3}Mn_{1/3}O_2$	2-4.1 V	0.1557%, 150, 750	Chem. Eng. J. 2024[25]
	P2-$Na_{0.67}Ni_{0.33}Mn_{0.59}Cu_{0.08}O_{1.95}F_{0.05}$	2-4.3 V	0.0936%, 500, 600	Small 2025[26]
	O3-$Na_{0.93}Li_{0.12}Ni_{0.25}Fe_{0.15}Mn_{0.48}O_2$	2-4.2 V	0.086%, 200, 1600	Adv. Funct. Mater. 2022[27]
	O3-$Na_{0.95}Ni_{0.40}Fe_{0.15}Mn_{0.3}Ti_{0.15}O_2$	2-4.2 V	0.091%, 200, 1000	ACS Appl. Mater. Interfaces 2023[28]
	P2-$Na_{0.67}Ni_{0.326}Mn_{0.653}La_{0.02}O_2$	2-4.0 V	0.0582%, 500, 1500	ACS Energy Lett. 2025[29]
	O3-$NaNi_{0.25}Fe_{0.14}Mn_{0.3}Li_{0.1}Ti_{0.15}$-$Cu_{0.03}Zn_{0.03}O_{1.94}F_{0.06}$	2-4.2 V	0.0946%, 200, 150; 0.0713%, 500, 750; 0.0538%, 500, 1500	This work
High temperature	O3-$NaNi_{0.4}Cu_{0.05}Mg_{0.05}Mn_{0.3}Ti_{0.2}O_2$	2-4.0 V	0.261%, 100, 75, 55 °C	Chem. Sci. 2025[30]
	O3-$NaNi_{0.5}Mn_{0.48}La_{0.02}O_2$	2-4.0 V	0.125%, 100, 150, 55 °C	Angew. Chem. Int. Ed. 2025[31]
	O3-$Na_{0.9}Ca_{0.03}Ni_{0.33}Fe_{0.33}Mn_{0.30}Sn_{0.03}O_2$	2-4.2 V	0.179%, 100, 150, 50 °C	J. Am. Chem. Soc. 2026[32]
	O3-$Na_{0.95}Ni_{0.3}Mn_{0.5}Cu_{0.1}Li_{0.05}Ti_{0.05}O_2$	2-4.2 V	0.11%, 100, 150, 40 °C	Energy Storage Mater. 2025[33]
	O3-$NaNi_{0.4}Mg_{0.05}Cu_{0.05}Mn_{0.3}Ti_{0.2}B_{0.05}O_2$	2-4.3 V	0.21%, 50, 32, 55 °C	Angew. Chem. Int. Ed. 2026[34]
	O3-$Na_{0.9}Ca_{0.05}Cu_{0.15}Ni_{0.25}Mn_{0.4}Ti_{0.1}Sn_{0.05}O_2$	2-4.2 V	0.1865%, 200, 75, 40 °C	Adv. Energy Mater. 2026[35]

	$P2\text{-}Na_{0.67}Ni_{0.326}Mn_{0.653}La_{0.02}O_2$	2-4.3 V	0.189%, 100, 750, 60 °C	ACS Energy Lett. 2025[29]
	$O3\text{-}NaNi_{0.25}Fe_{0.14}Mn_{0.3}Li_{0.1}Ti_{0.15}\text{-}Cu_{0.03}Zn_{0.03}O_{1.94}F_{0.06}$	2-4.2 V	0.1208%, 300, 750, 60 °C	This work
Low temperature	$O3\text{-}NaNi_{0.5}Mn_{0.48}La_{0.02}O_2$	2-4.0 V	0.072%, 150, 15, -20 °C	Adv. Funct. Mater. 2025[19]
	$O3\text{-}NaNi_{0.5}Mn_{0.49}Sb_{0.01}O_2$	2-4.0 V	0.09%, 100, 15, -20 °C	ACS Nano 2022[36]
	$O3\text{-}Na[Ni_{0.4}Cu_{0.1}Mn_{0.4}Ti_{0.1}]O_2@NaCaPO_4$	2-4.2 V	0.0495%, 200, 75, -10 °C	Nat. Commun. 2025[37]
	$O3\text{-}NaNi_{0.25}Fe_{0.14}Mn_{0.3}Li_{0.1}Ti_{0.15}\text{-}Cu_{0.03}Zn_{0.03}O_{1.94}F_{0.06}$	2-4.2 V	0.05%, 200, 75, -20 °C	This work

1

2

Table S7. Summary of the electrochemical performance (initial specific capacity) of layered oxides for sodium-ion batteries.

Temperature	Materials	Voltage region (V)	Initial specific capacity (mAh g^{-1}), Current density (mA g^{-1})	Ref.
Room temperature	O3-$Na_{0.9}Ni_{0.32}Zn_{0.08}Fe_{0.1}Mn_{0.3}Ti_{0.2}O_2$	2-4.2 V	140, 150	Angew. Chem. Int. Ed. 2024[17]
	O3-$NaNi_{0.4}Fe_{0.2}Mn_{0.4}O_2$@2%$Na_{0.44}MnO_2$	2-4.3 V	140, 160	J. Am. Chem. Soc. 2024[38]
	O3-$Na[Ni_{0.3}Mn_{0.5}Cu_{0.1}Ti_{0.1}]O_2$	2-4.3 V	135, 120	ACS Nano 2025[39]
	O3-$Na[Ni_{0.4}Cu_{0.1}Mn_{0.4}Ti_{0.1}]O_2$@$NaCaPO_4$	2-4.2 V	130.1, 150	Nat. Commun. 2025[37]
	O3-$NaCu_{0.1}Ni_{0.25}Co_{0.15}Mn_{0.35}Li_{0.05}Ti_{0.05}Sn_{0.05}O_2$	2-4.4 V	122.8, 150	Angew. Chem. Int. Ed. 2025[22]
	O3-$NaNi_{0.3}Mn_{0.5}Fe_{0.05}Li_{0.05}Ti_{0.05}Cu_{0.05}O_2$	2-4.2 V	120, 150	Adv. Energy Mater. 2025[14]
	O3-$NaNi_{0.25}Mg_{0.05}Cu_{0.1}Fe_{0.2}Mn_{0.2}Ti_{0.1}Sn_{0.1}O_2$	2-4.0 V	120, 140	J. Am. Chem. Soc. 2022[40]
	O3-$Na[Ni_{1/3}Fe_{1/3}Mn_{1/3}]_{0.99}Sc_{0.01}O_2$	2-4.2 V	119.6, 130	Adv. Funct. Mater. 2024[16]
	O3-$NaNi_{0.35}Mn_{0.35}Cu_{0.1}Fe_{0.1}Ti_{0.05}Sn_{0.05}O_2$	2-4.15 V	115, 120	Nat. Commun. 2025[41]
	O3-$Na_{0.8}Ni_{0.3}Fe_{0.2}Mn_{0.3}Li_{0.1}Mg_{0.02}Ca_{0.05}Sb_{0.03}O_2$	2-4.2 V	110, 140	Adv. Energy Mater. 2023[42]
	O3-$Na_{0.55}Mn_{0.4}Ni_{0.3}Fe_{0.15}Li_{0.1}Ti_{0.05}O_2$	2-4.2 V	102, 120	Nat. Commun. 2025[43]
	O3-$NaNi_{1/3}Fe_{1/3}Mn_{1/3}O_2$	2-4.1 V	137, 750	Chem. Eng. J. 2024[25]
	O3-$Na_{2/3}Li_{1/6}Fe_{1/6}Co_{1/6}Ni_{1/6}Mn_{1/3}O_2$	2-4.5 V	111, 750	Adv. Energy Mater. 2022[24]
	P2/O3-$Na_{0.7}Ni_{0.2}Fe_{0.2}Mn_{0.5}Zn_{0.1}O_2$	2.4-4.5 V	106.9, 600	ACS Nano 2024[23]
	P2-$Na_{0.67}Ni_{0.33}Mn_{0.59}Cu_{0.08}O_{1.95}F_{0.05}$	2-4.3 V	106.3, 600	Small 2025[26]
	P2/O3-$Na_{0.7}Mn_{0.53}Ni_{0.26}Fe_{0.15}$-$Mg_{0.01}V_{0.01}Co_{0.01}Cu_{0.01}Zn_{0.01}Sn_{0.01}O_2$	2.1-4.3 V	85, 750	Angew. Chem. Int. Ed. 2025[44]
	P2/O3-$Na_{0.8}Mg_{0.06}Ni_{0.34}Mn_{0.54}Ti_{0.06}O_2$	2-4.4 V	110, 2000	Adv. Funct. Mater. 2025[45]
	O3-$Na_{0.9}Ni_{0.25}Zn_{0.07}Fe_{0.28}Co_{0.08}Mn_{0.15}Ti_{0.17}O_2$	2-4.1 V	101.2, 1500	Adv. Funct. Mater. 2025[46]
	O3-$Na_{0.93}Li_{0.12}Ni_{0.25}Fe_{0.15}Mn_{0.48}O_2$	2-4.2 V	99.2, 1600	Adv. Funct. Mater. 2022[27]
	P2-$Na_{0.75}[Ni_{0.3}Mn_{0.5}Cu_{0.1}Ti_{0.05}Mo_{0.05}]O_2$	2-4.3 V	95.34, 1500	Adv. Funct. Mater. 2025[47]
	O3-$Na_{0.9}Ca_{0.05}Cu_{0.15}Ni_{0.25}Mn_{0.4}Ti_{0.1}Sn_{0.05}O_2$	2-4.2 V	85, 1000	Adv. Energy Mater. 2026[35]
	P2-$Na_{0.67}Ni_{0.326}Mn_{0.653}La_{0.02}O_2$	2-4.0 V	75, 1730	ACS Energy Lett. 2025[29]
	O3-$NaNi_{0.25}Fe_{0.14}Mn_{0.3}Li_{0.1}Ti_{0.15}$-$Cu_{0.03}Zn_{0.03}O_{1.94}F_{0.06}$	2-4.2 V	146.8, 150; 141.04, 750; 129.68, 1500	This work
High temperature	O3-$Na_{0.95}Ni_{0.3}Mn_{0.5}Cu_{0.1}Li_{0.05}Ti_{0.05}O_2$	2-4.2 V	152.7, 15, 40°C	Energy Storage Mater. 2025[33]

	$O3\text{-}NaNi_{0.4}Mg_{0.05}Cu_{0.05}Mn_{0.3}Ti_{0.2}B_{0.05}O_2$	2-4.3 V	137, 16, 55°C	Angew. Chem. Int. Ed. 2026[34]
	$O3\text{-}Na[Ni_{0.4}Cu_{0.1}Mn_{0.4}Ti_{0.1}]O_2@NaCaPO_4$	2-4.2 V	139.55, 75, 50°C	Nat. Commun. 2025[37]
	$O3\text{-}Na_{0.9}Ca_{0.05}Cu_{0.15}Ni_{0.25}Mn_{0.4}Ti_{0.1}Sn_{0.05}O_2$	2-4.2 V	106, 75, 40°C	Adv. Energy Mater. 2026[35]
	$P2\text{-}Na_{0.67}Ni_{0.326}Mn_{0.653}La_{0.02}O_2$	2-4.3 V	83, 865, 60°C	ACS Energy Lett. 2025[29]
	$O3\text{-}NaNi_{0.25}Fe_{0.14}Mn_{0.3}Li_{0.1}Ti_{0.15}\text{-}Cu_{0.03}Zn_{0.03}O_{1.94}F_{0.06}$	2-4.2 V	155.43, 30, 60°C 143.47, 750, 60°C	This work
Low temperature	$O3\text{-}NaNi_{0.5}Mn_{0.49}Sb_{0.01}O_2$	2-4.0 V	122.3, 15, -20 °C	ACS Nano 2022[36]
	$O3\text{-}NaNi_{0.5}Mn_{0.48}La_{0.02}O_2$	2-4.0 V	115, 15, -20°C	Adv. Funct. Mater. 2025[19]
	$O3\text{-}Na_{0.9}Ca_{0.05}Cu_{0.15}Ni_{0.25}Mn_{0.4}Ti_{0.1}Sn_{0.05}O_2$	2-4.2 V	78, 75, -20°C	Adv. Energy Mater. 2026[35]
	$O3\text{-}Na[Ni_{0.4}Cu_{0.1}Mn_{0.4}Ti_{0.1}]O_2@NaCaPO_4$	2-4.2 V	129.6, 15, -10°C 110, 75, -10°C	Nat. Commun. 2025[37]
	$O3\text{-}NaNi_{0.25}Fe_{0.14}Mn_{0.3}Li_{0.1}Ti_{0.15}\text{-}Cu_{0.03}Zn_{0.03}O_{1.94}F_{0.06}$	2-4.2 V	122.5, 15, -20°C 111.74, 75, -20°C	This work

Reference:

Y. Dong, Z. Zhou, Y. Ma, H. Zhang, F. Meng, Y. Wu, Y. Ma, *ACS Energy Lett.* 2024, **9**, 5096-5119.

G. Kresse, J. Furthmüller, *Phys. Rev. B* 1996, **54**, 11169-11186.

J. Perdew, K. Burke, M. Ernzerhof, *Phys. Rev. Lett.* 1996, **77**, 3865-3868.

M. Ernzerhof, G. Scuseria, *J. Chem. Phys.* 1999, **110**, 5029-5036.

Z. Chen, Y. Chen, H. Hu, H. Zhu, Y. Ji, Z. Huang, Y. Wang, J. Duan, *J. Alloys Compd.* 2025, **1025**, 180310.

Z. Li, W. Xi, Z. Jiang, Y. Zhang, R. Wang, Y. Gong, H. Wang, J. Jin, *Small* 2025, **21**, e06854.

J. Zhan, J. Huang, Z. Li, J. Yuan, S. Dou, H. Liu, C. Wu, *Nano Lett.* 2024, **24**, 9793-9800.

F. Ding, H. Wang, Q. Zhang, L. Zheng, H. Guo, P. Yu, N. Zhang, Q. Guo, F. Xie, R. Dang, X. Rong, Y. Lu, R. Xiao, L. Chen, Y. Hu, *J. Am. Chem. Soc.* 2023, **145**, 13592-13602.

S. Grimme, J. Antony, S. Ehrlich, H. Krieg, *J. Chem. Phys.* 2010, **132**, 154104.

S. Grimme, S. Ehrlich, L. Goerigk, *J. Comput. Chem.* 2011, **32**, 1456-1465.

V. Wang, N. Xu, J. Liu, G. Tang, W. Geng, *Comput. Phys. Commun.* 2021, **267**, 108033.

K. Momma, F. Izumi, *J. Appl. Crystallogr.* 2011, **44**, 1272-1276.

J. Nørskov, T. Bligaard, A. Logadottir, J. Kitchin, J. Chen, S. Pandelov, U. Stimming, *J. Electrochem. Soc.* 2005, **152**, J23.

H. Bi, X. Sun, B. Zhao, R. Li, Y. Zhang, X. Wang, M. Zhang, D. Luo, Z. Chen, *Adv. Energy Mater.* 2025, **15**, 2501229.

L. Zhang, Y. Hong, J. Xu, S. Lin, Z. Lin, L. Zheng, H. Yao, Z. Hong, *Energy Storage Mater.* 2025, **82**, 104556.

N. Hong, J. Li, H. Wang, X. Hu, B. Zhao, F. Hua, Y. Mei, J. Huang, B. Zhang, W. Jian, J. Gao, Y. Tian, X. Shi, W. Deng, G. Zou, H. Hou, Z. Hu, Z. Long, X. Ji, *Adv. Funct. Mater.* 2024, **34**, 2402398.

T. Zhang, M. Ren, Y. Huang, F. Li, W. Hua, S. Indris, F. Li, *Angew. Chem. Int. Ed.* 2024, **63**, e202316949.

F. Ding, P. Ji, Z. Han, X. Hou, Y. Yang, Z. Hu, Y. Niu, Y. Liu, J. Zhang, X. Rong, Y. Lu, H. Mao, D. Su, L. Chen, Y. Hu, *Nat. Energy* 2024, **9**, 1529-1539.

T. Yuan, P. Li, Y. Sun, H. Che, Q. Zheng, Y. Zhang, S. Huang, J. Qiu, Y. Pang, J. Yang, Z. Ma, S. Zheng, *Adv. Funct. Mater.* 2025, **35**, 2414627.

J. Yao, X. Wang, P. Hu, J. Fan, X. Yang, W. Jiang, S. Jiang, P. Dong, Y. Zhang, J. Duan, Z. Zhou, *Adv. Funct. Mater.* 2024, DOI: 10.1002/adfm.202419967.

C. Cai, X. Li, J. Li, R. Yu, P. Hu, T. Zhu, T. Li, S. Lee, N. Xu, H. Fan, J. Wu, L. Zhou, L. Mai, K. Amine, *Nat. Commun.* 2025, **16**, 100.

H. Wang, J. Gao, Y. Mei, L. Ni, Y. He, N. Hong, J. Huang, W. Deng, G. Zou, H. Hou, T. Liu, C. Liang, X. Ji, K. Amine, *Angew. Chem. Int. Ed.* 2025, **64**, e202418605.

H. Wang, H. Chen, Y. Mei, J. Gao, L. Ni, N. Hong, B. Zhang, F. Zhu, J. Huang, K. Wang, W. Deng, D. Silvester, C. Banks, S. Yasar, B. Song, G. Zou, H. Hou, X. Ji, *ACS Nano* 2024, **18**, 13150-13163.

L. Yao, P. Zou, C. Wang, J. Jiang, L. Ma, S. Tan, K. Beyer, F. Xu, E. Hu, H. Xin, *Adv. Energy Mater.* 2022, **12**, 2201989.

J. Wang, F. Xu, X. Fan, C. Zheng, Y. Zhao, L. Zuo, X. Yun, D. Lu, P. Xiao, Y. Chen, *Chem. Eng. J.* 2024, **500**, 157032.

X. Zhang, F. Xie, J. Han, X. Wang, T. Liu, J. Yu, L. Zhang, *Small* 2025, **21**, 2502292.

X. Yuan, Y. Guo, L. Gan, X. Yang, W. He, X. Zhang, Y. Yin, S. Xin, H. Yao, Z. Huang, Y. Guo, *Adv. Funct. Mater.* 2022, **32**, 2111466.

L. Yu, Y. Chang, M. Liu, Y. Feng, D. Si, X. Zhu, X. Wang, P. Wang, S. Xu, *ACS Appl. Mater. Interfaces* 2023, **15**, 23236-23245.

Z. Song, S. Kansara, S. Cheng, M. Yang, F. Li, C. Qi, S. Li, J. Hwang, Y. Bai, *ACS Energy Lett.* 2025, **10**, 5199-5208.

Y. Wu, H. Hu, J. Li, H. Dong, Y. Zhu, S. Chen, N. Wang, J. Wang, Y. Xiao, *Chem. Sci.* 2025, **16**, 3928-3937.

J. Kuang, Z. Liu, L. Fu, Y. Shi, M. Zhang, Y. Wang, N. Ding, D. Sun, Y. Tang, H. Wang, *Angew. Chem. Int. Ed.* 2025, **64**, e202500715.

K. Zhang, J. Zou, Z. Xu, G. Liu, L. He, Q. Yu, F. Wang, Y. Xia, *J. Am. Chem. Soc.* 2025, **147**, 48147-48157.

X. Wang, H. Li, Z. Dai, J. Li, Y. Song, B. Han, X. Wang, J. Chen, C. Dong, Z. Mao, L. Zhang, *Energy Storage Mater.* 2025, **79**, 104345.

H. Hu, M. Yang, D. Chen, N. Xu, J. Li, Y. Zhu, Y. Wu, H. Dong, J. Wang, C. Yao, Y. Yan, S. Chen, N. Wang, W. K. Pang, Y. Sun, J. Wang, Y. Xiao, *Angew. Chem. Int. Ed.* 2026, **65**, e19108.

W. Xu, C. Cheng, L. Wang, T. Chen, Z. Zhou, T. Yan, S. Shen, P. Zeng, L. Zhang, *Adv. Energy Mater.* 2026, **16**, e04557.

T. Yuan, S. Li, Y. Sun, J. Wang, A. Chen, Q. Zheng, Y. Zhang, L. Chen, G. Nam, H. Che, J. Yang, S. Zheng, Z. Ma, M. Liu, *ACS Nano* 2022, **16**, 18058-18070.

X. Liang, X. Song, H. H. Sun, H. Kim, M. Kim, Y. Sun, *Nat. Commun.* 2025, **16**, 3505.

L. Kong, J. Li, H. Liu, Y. Zhu, J. Wang, Y. Liu, X. Zhang, H.-Y. Hu, H. Dong, Z. Jian, C. Cheng, S. Chen, L. Zhang, J. Wang, S. Chou, Y. Xiao, *J. Am. Chem. Soc.* 2024, **146**, 32317-32332.

D. Yang, L. Chen, X. Gao, Z. Zhao, Q. Lai, H. Chen, Y. Long, Q. Gu, Z. Liu, W. Luo, *ACS Nano* 2025, **19**, 2834-2847.

F. Ding, C. Zhao, D. Xiao, X. Rong, H. Wang, Y. Li, Y. Yang, Y. Lu, Y. Hu, *J. Am. Chem. Soc.* 2022, **144**, 8286-8295.

[141] H. Wang, T. Liu, H. Chen, Y. Mei, J. Gao, L. Ni, N. Hong, J. Huang, X. Hu, W. Deng, G. Zou, H. Hou, D. Silvester, C. Banks, X. Ji, K. Amine, *Nat. Commun.* 2025, **16**, 4409.
[142] K. Zhang, Z. Xu, G. Li, R. Luo, C. Ma, Y. Wang, Y. Zhou, Y. Xia, *Adv. Energy Mater.* 2023, **13**, 2302793.
[143] M. Li, H. Zhuo, J. Lei, Y. Guo, Y. Yuan, K. Wang, Z. Liao, W. Xia, D. Geng, X. Sun, J. Hu, B. Xiao, *Nat. Commun.* 2025, **16**, 2010.
[144] Z. Huang, T. Yang, J. Cao, K. Zhang, Y. Liu, B. Xin, K. Xu, Y. Liu, X. Zhou, J. Guo, T. Wang, H. Geng, X. Wu, *Angew. Chem. Int. Ed.* 2025, **64**, e202505367.
[145] S. Sun, X. Zhu, H. Dong, Y. Feng, Y. Tang, M. Li, S. Xu, H. Xin, C. Ma, G. Wei, L. Hu, H. Qin, M. Liu, Y. Xiao, B. Xiao, P. Wang, *Adv. Funct. Mater.* 2025, **35**, 2503900.
[146] W. Qiu, Z. Chen, Z. Liu, W. Xu, K. Zhang, Y. Hou, J. Lu, X. Zhan, Y. Li, Q. Zhang, *Adv. Funct. Mater.* 2025, **35**, 2422106.
[147] Q. Lai, C. Liu, D. Yang, X. Gao, R. Yang, Q. Li, Z. Liu, Q. Gu, W. Luo, *Adv. Funct. Mater.* 2025, DOI: 10.1002/adfm.202516173.